Electronic Supplementary Information (ESI) for Chemical Communications. This journal is (c) The Royal Society of Chemistry 2024.
Electronic Supplementary Information (ESI)

Engineering a high-capacity and long-cycle life magnesium/lithium hybrid-ion battery using lamellar $SnSe_2/SnSe/SnO_2$ cathode

Jiamin Liu[a], Ting Zhou[a], Yun Shen[b], Peng Zuo[b], Hui Qiu[b], Yajun Zhu[a,c] and Jinyun Liu[a,*]

Experimental Section

Preparation of hierarchical SnO_2 precursor

Typically, 6.846 g sucrose and 3.506 g $SnCl_4 \cdot 5H_2O$ were dissolved in 40 mL deionized water, and the clear solution was poured into a 50 mL Teflon-lined autoclave and maintained at 180 °C for 6 h. After cooling down naturally to room temperature, the resulting brown precipitate was washed with deionized water and ethanol for several times, and dried at 60 °C. The sample was placed in a ceramic boat and calcined at 500 °C for 1 h with a ramping rate of 1 °C min^{-1} under air atmosphere.

Preparation of lamellar $SnSe_2/SnSe/SnO_2$

1.5 g of SnO_2 and 7.5 g of selenium powders were separately placed in two ceramic boats. The one containing selenium powders were placed at the upstream side and another at the center of the tube furnace. Then it was annealed at 500 °C for 2 h in an Ar/H_2 atmosphere.

Characterizations

The X-ray Powder diffraction (XRD) was performed using a Hitachi Smart Lab 9 KW (Japan) with Cu-Kα radiation over the 2θ range of 10-80°. The morphology of the composite was characterized by scanning electron microscopy (FESEM, Hitachi Regulus 8100, operated at 5 kV), and the distribution of elements was analyzed by energy dispersive spectroscopy (EDS). The microstructure and crystallinity of the sample was obtained by using transmission electron microscope (TEM, HT-7700) and

high-resolution TEM (HRTEM, JEM-2100F microscope, operated at 200 kV) images. Elemental (Sn, Se, O, and C) valence states were characterized by X-ray photoelectron spectroscopy (XPS, EscalAB 250). Raman spectra were obtained by using Raman spectroscopy (Renishaw in Via). And the Brunauer Emmett Teller (BET) specific surface area of the sample was measured by a surface area tester (ASAP Micromeritics Tristar 2460).

Electrochemical measurements

The as-prepared $SnSe_2$/SnSe/SnO_2 (80 wt%), acetylene black (10 wt.%) and polyvinylidene fluoride (6.54% PVDF, 10 wt%) were dissolved in N-methyl pyrrolidinone (NMP). The slurry was uniformly spread on copper foil and dried under vacuum for 24 h at 80°C. The electrode sheet with an area of 2 cm^2 was obtained by a punch. And the electrode has a mass load of about 0.8-1.3 mg cm^{-2} of the active materials. The coin cells (CR2032) were assembled with $SnSe_2$/SnSe/SnO_2 as the cathode, polished Mg foil as anode and glass fiber film (Whatman, GF/F) separator in glovebox. An 0.4 mol L^{-1} all-phenyl composite (APC) with 0.4 mol L^{-1} lithium chloride (LiCl) was prepared as electrolyte for MLHBs. The galvanostatic charge-discharge was tested on a Neware battery test system. Cyclic voltammetry (CV) curves and electrochemical impedance spectroscopy (EIS) spectra were measured by using an electrochemical workstation (CHI 660E).

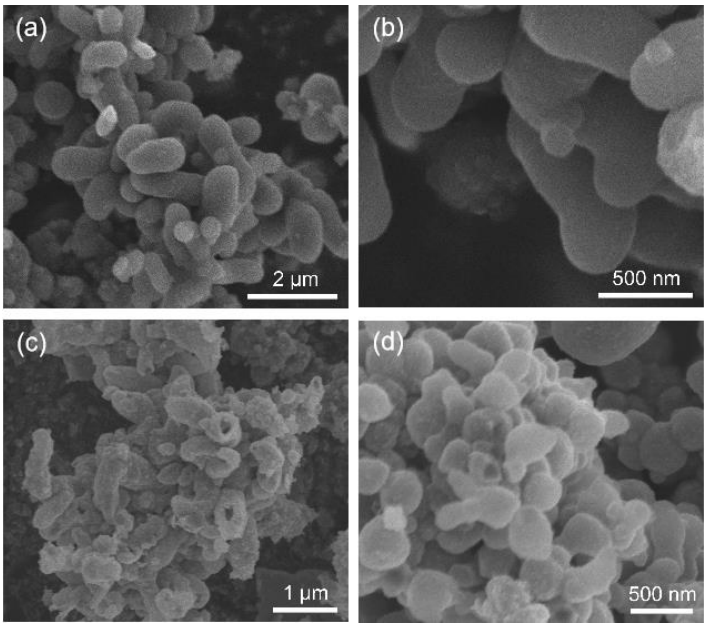

Fig. S1 SEM images of (a, b) hierarchical SnO_2@C and (c, d) SnO_2.

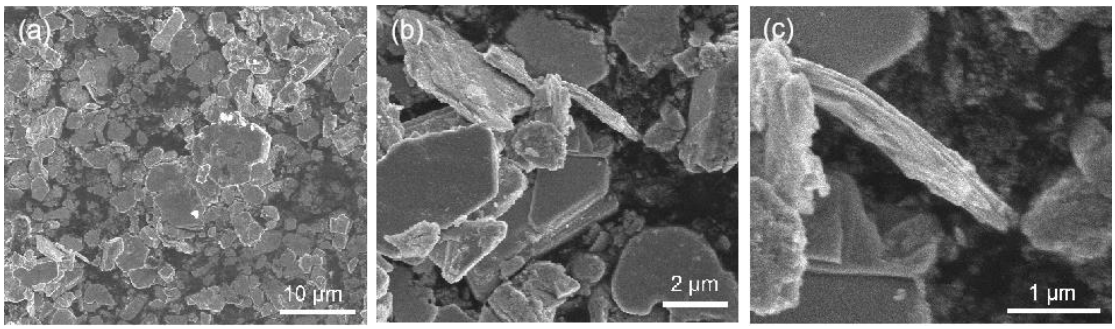

Fig. S2 (a-c) SEM images of $SnSe_2$/SnSe/SnO_2.

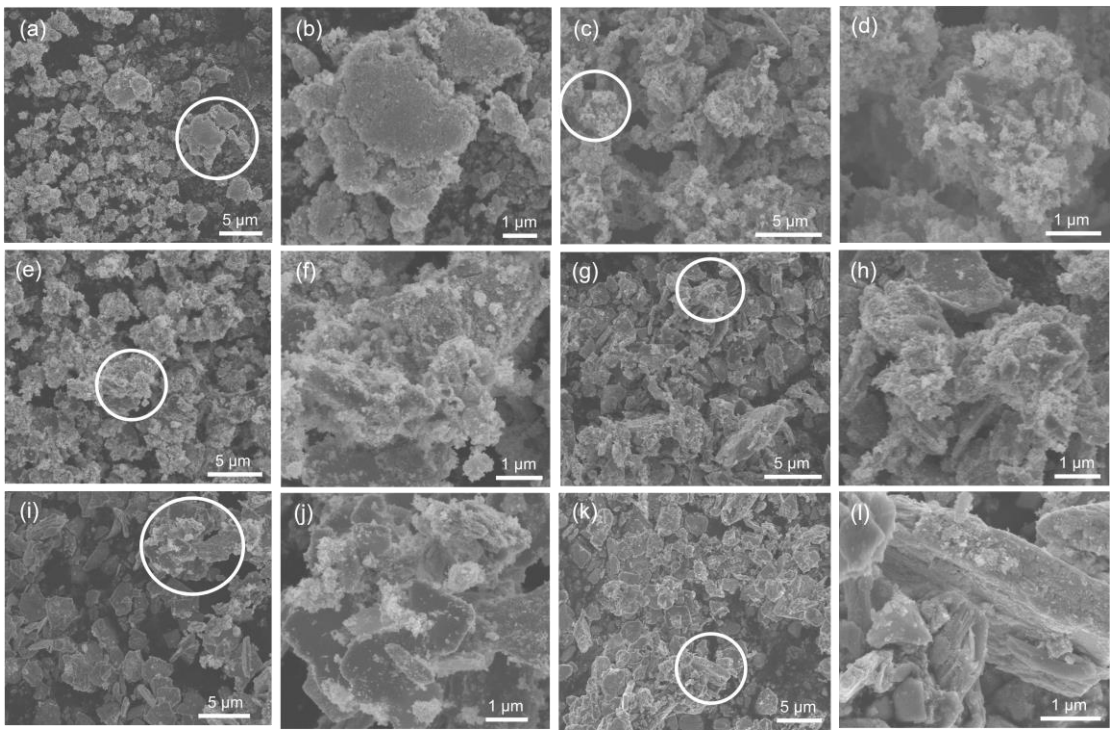

Fig. S3 SEM images of samples after selenization for (a, b) 10, (c, d) 20, (e, f) 30, (g, h) 40, (i, j) 60 and (k, l) 90 min.

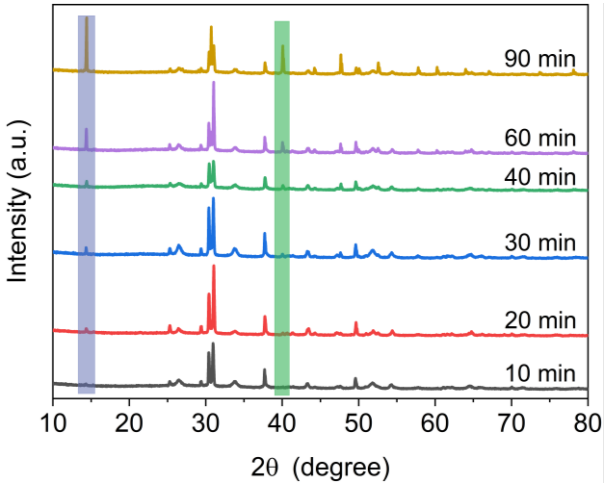

Fig. S4 XRD patterns of the samples after different selenization times.

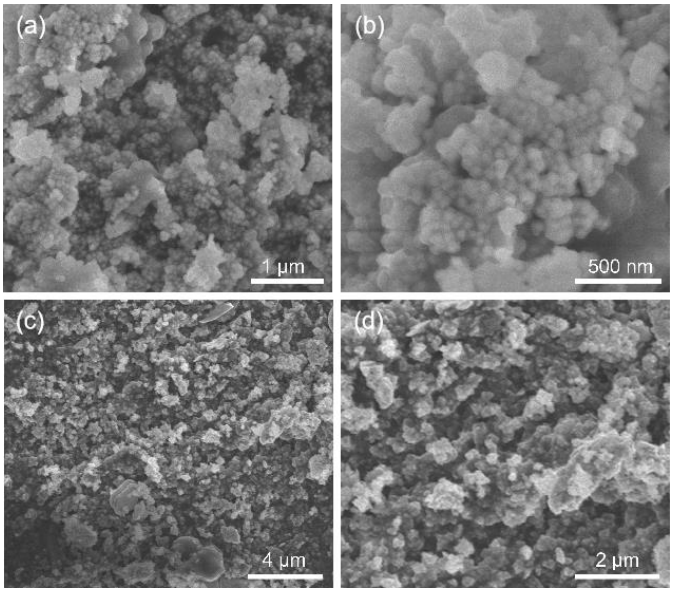

Fig. S5 SEM images of (a, b) SnO_2 particles and (c, d) as-formed $SnSe_2$/SnSe/SnO_2.

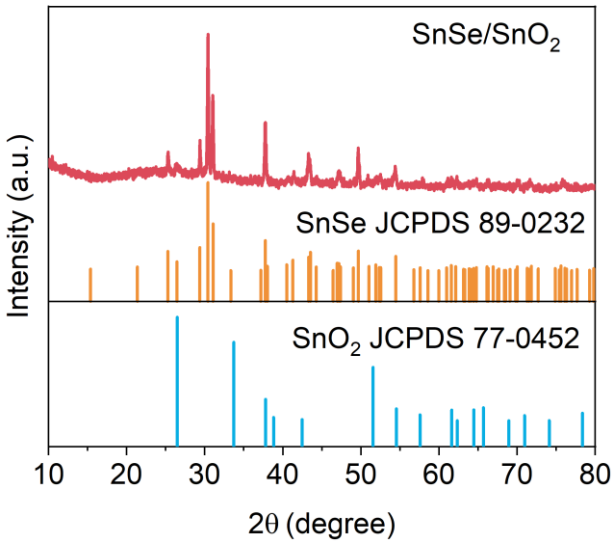

Fig. S6 XRD patterns of the granular SnSe/SnO_2.

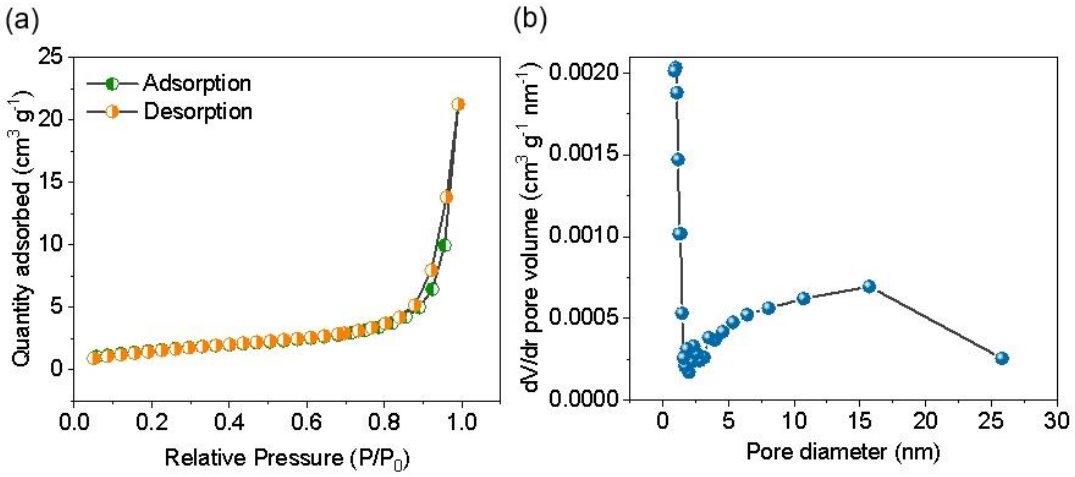

Fig. S7 (a) N_2 adsorption-desorption isotherms and (b) pore-size distribution of $SnSe_2/SnSe/SnO_2$.

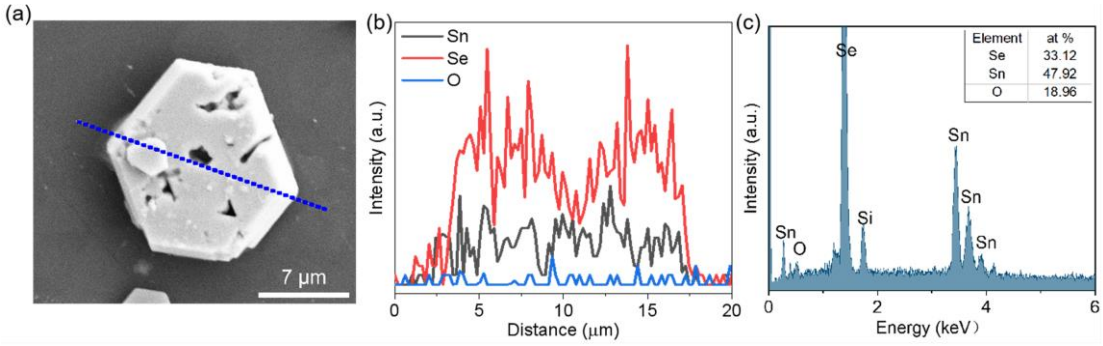

Fig. S8 (a) SEM image, (b) line-scanning curves and (c) EDS spectrum of $SnSe_2/SnSe/SnO_2$.

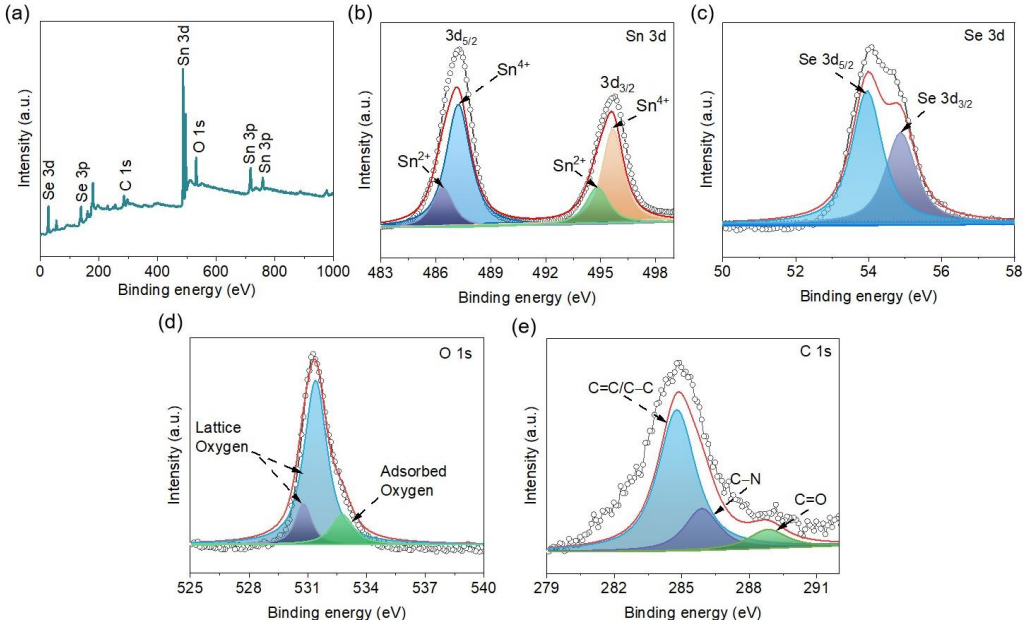

Fig. S9 (a) Survey spectrum of $SnSe_2/SnSe/SnO_2$. XPS spectra of $SnSe_2/SnSe/SnO_2$: (b) Sn 3d, (c) Se 3d, (d) O 1s and (e) C 1s.

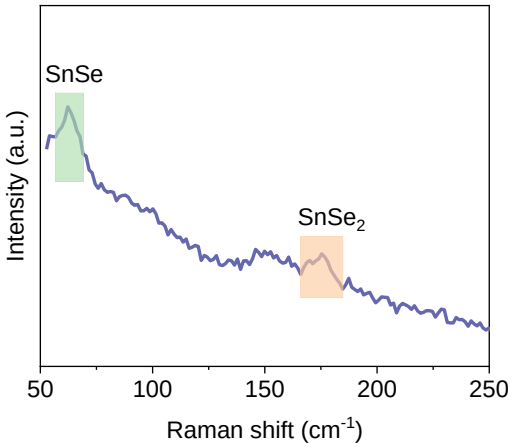

Fig. S10 Raman spectrum of $SnSe_2/SnSe/SnO_2$.

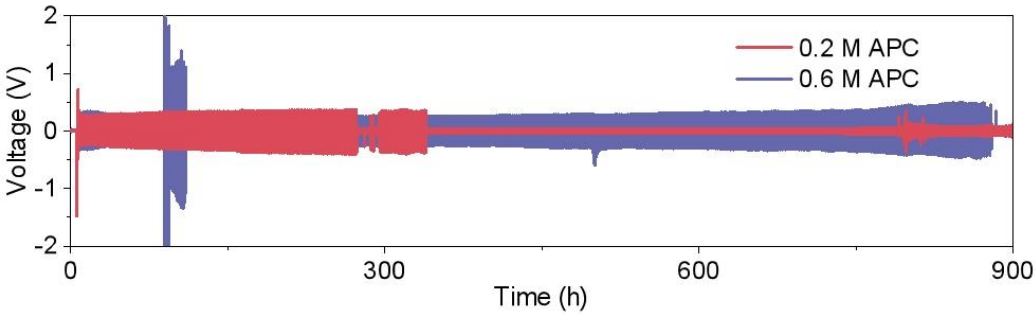

Fig. S11 Long-term Mg stripping/plating of the Mg|Mg cells using different concentrations of APC at 0.4 mA cm^{-2}.

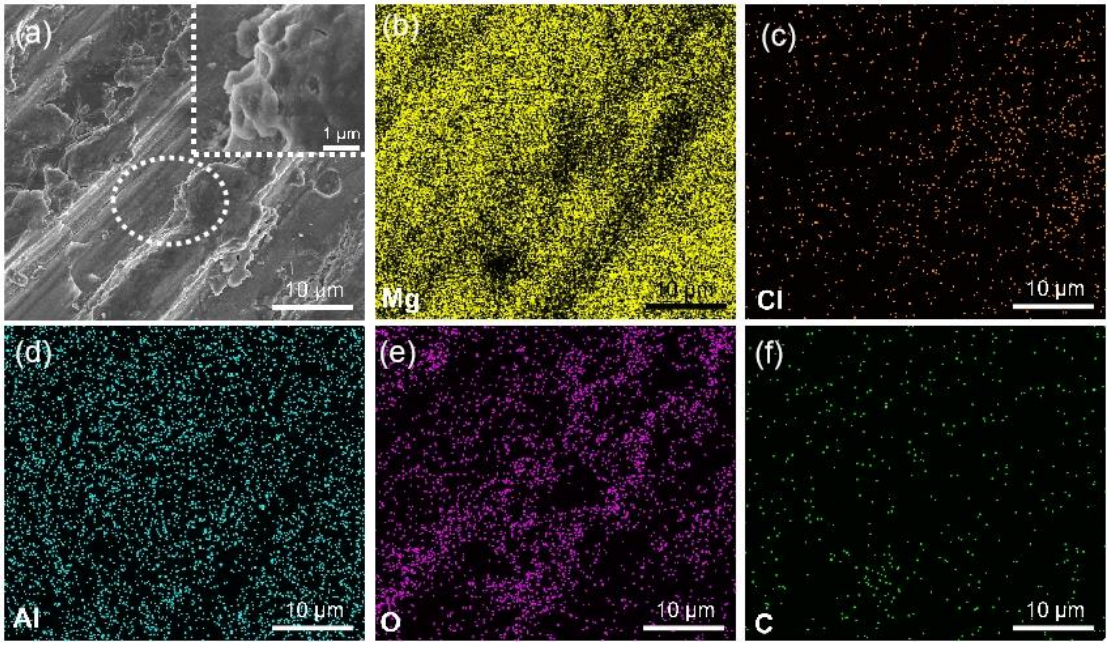

Fig. S12 (a) SEM image of Mg anode after cycling in the APC-0.2 M LiCl electrolyte and corresponding mapping images of (b) Mg, (c) Cl, (d) Al, (e) O and (f) C.

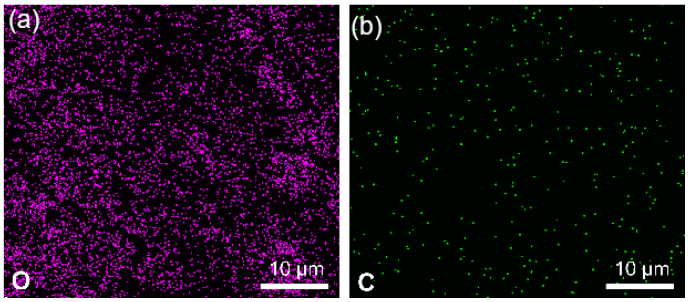

Fig. S13 Elemental mapping images of Mg anode after cycling in the APC-0.4 M LiCl electrolyte: (a) O and (b) C.

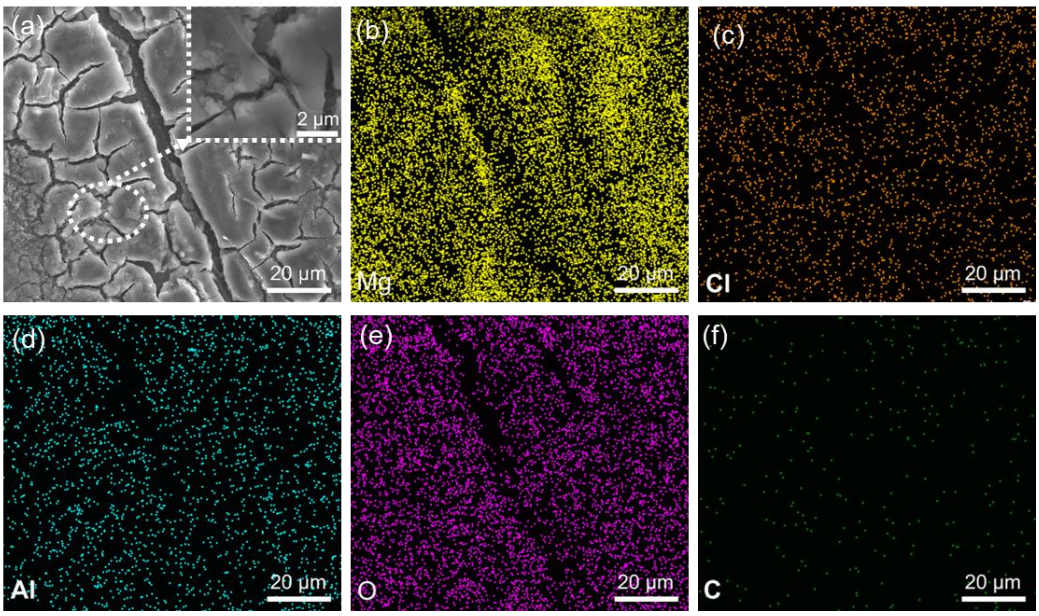

Fig. S14 (a) SEM image of Mg anode after cycling in the APC-0.6 M LiCl electrolyte and corresponding mapping images of (b) Mg, (c) Cl, (d) Al, (e) O and (f) C.

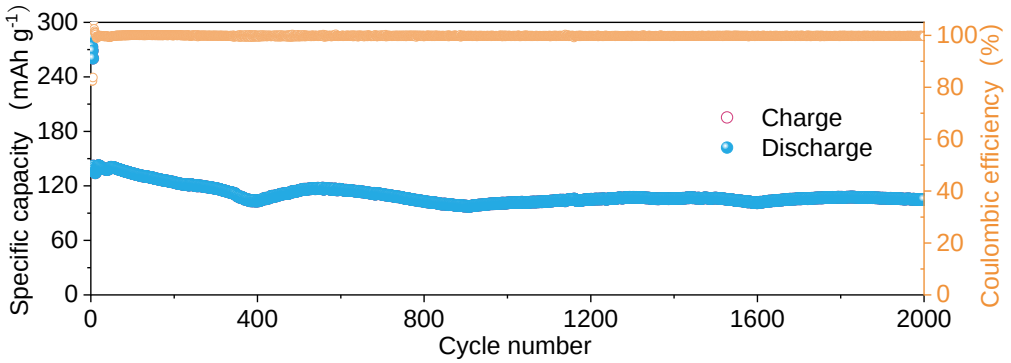

Fig. S15 Cycling performance of MLHB with $SnSe_2$/SnSe/SnO_2@C cathode working with APC-0.4 M LiCl electrolyte at 1.0 A g^{-1}.

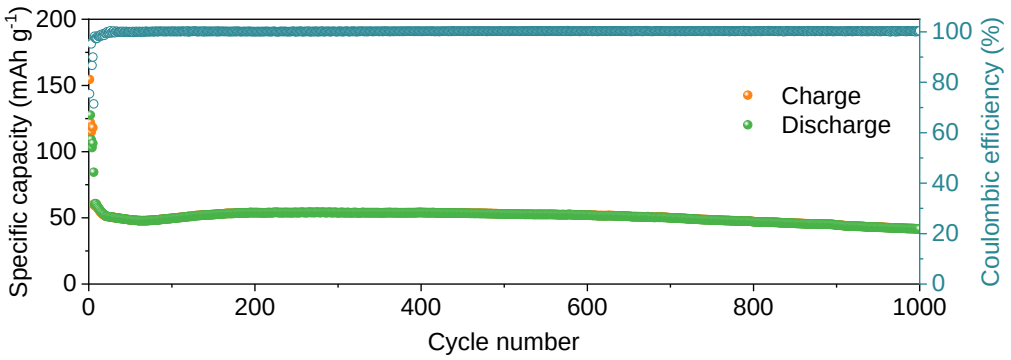

Fig. S16 Cycling performance of MLHB with SnSe/SnO_2 particles as cathode working with APC-0.4 M LiCl electrolyte at 1.0 A g^{-1}.

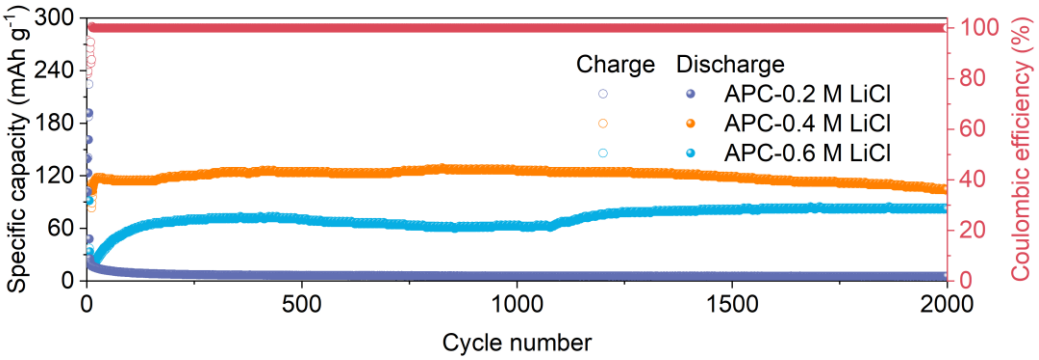

Fig. S17 Cycling performance of the MLHBs with lamellar $SnSe_2/SnSe/SnO_2$ as cathode and APC-x LiCl (x=0.2, 0.4 and 0.6 M) as electrolytes at 5.0 A g^{-1}.

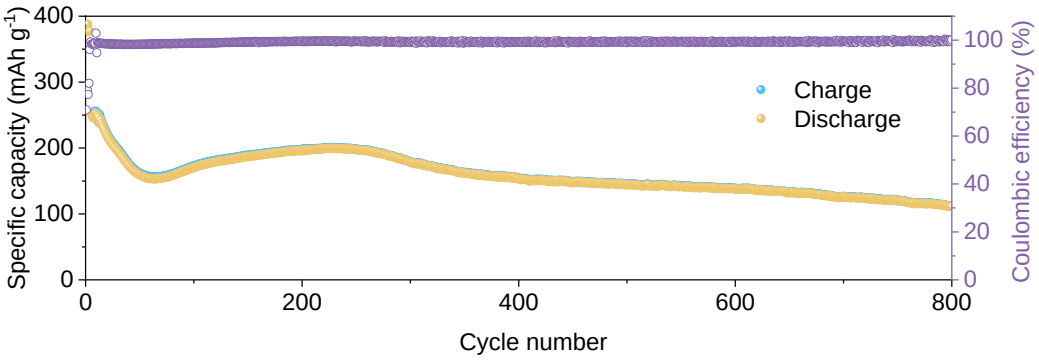

Fig. S18 Cycling performance of MLHB with $SnSe_2/SnSe/SnO_2$ cathode working with APC-0.4 M LiCl at 1.0 A g^{-1} under 50 °C. Before the cell was cycled at 1.0 A g^{-1}, a pre-activation for 5 cycles at 0.2 A g^{-1} was performed.

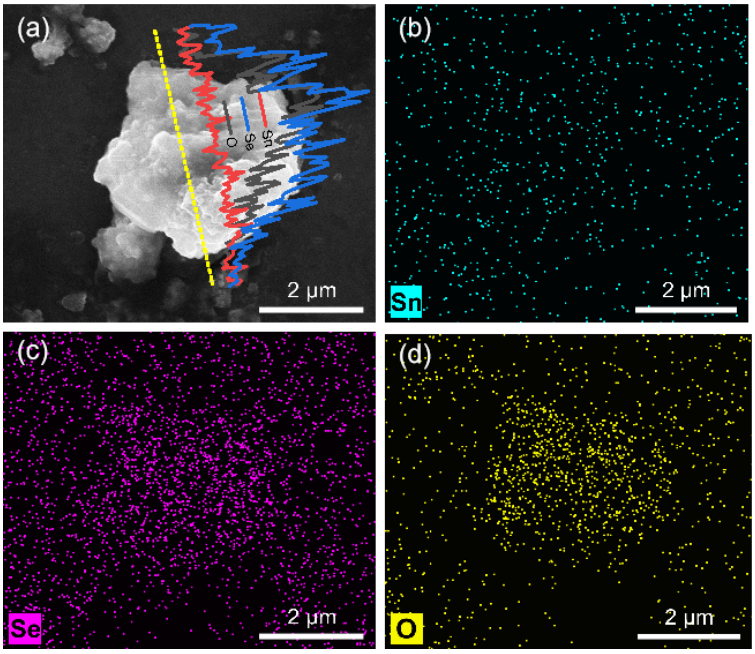

Fig. S19 (a) SEM image and line-scanning curves. (b) Mapping images of $SnSe_2/SnSe/SnO_2$ after cycling 500 times at 1.0 A g^{-1}.

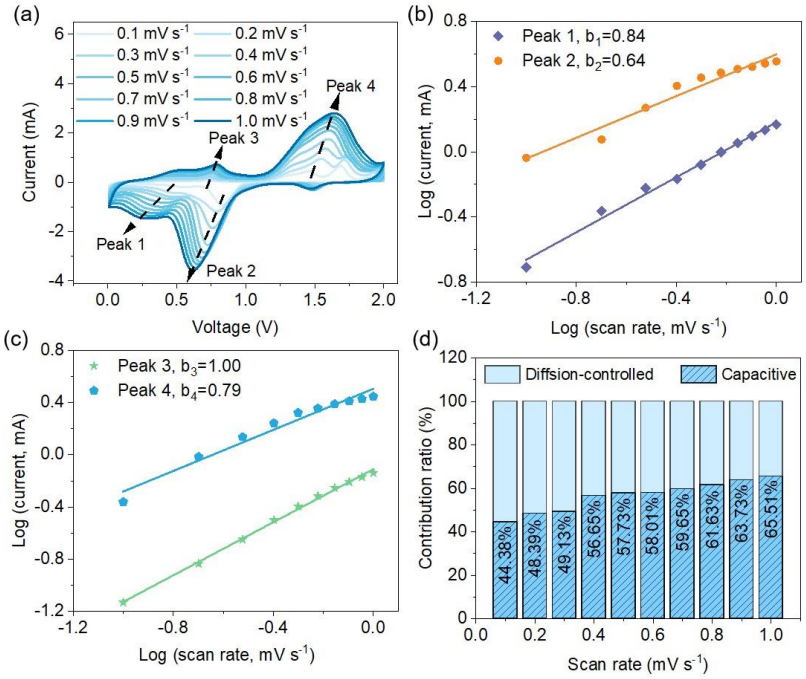

Fig. S20 (a) CV curves of the $SnSe_2/SnSe/SnO_2$-based MLHBs at scanning rates from 0.1 to 1.0 mV s^{-1}. (b, c) The log(i) versus log(v) plots. (d) The contribution ratios of capacitive and diffusion-controlled processes.

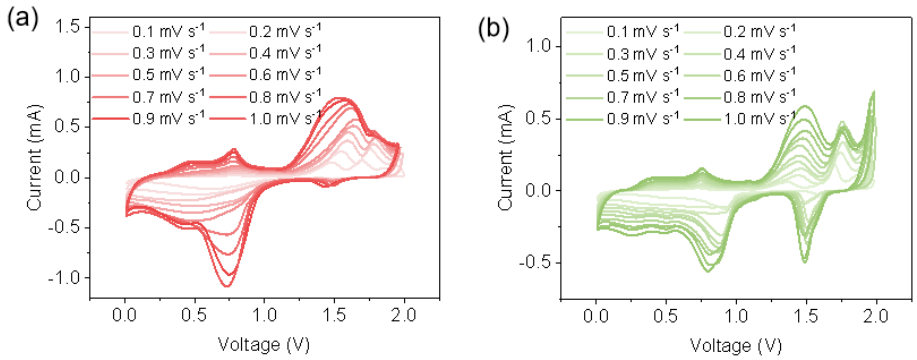

Fig. S21 CV curves of MLHBs using (a) APC-0.2 M LiCl and (b) APC-0.6 M LiCl electrolytes under scanning rates from 0.1 to 1.0 mV s^{-1}.

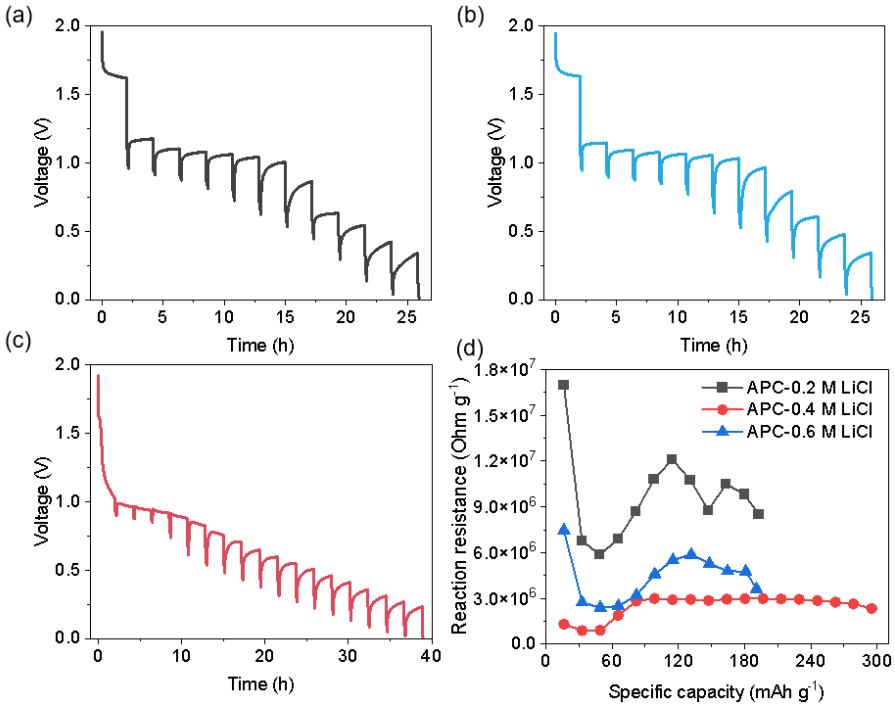

Fig. S22 GITT time-potential distributions of batteries with (a) APC-0.2 M LiCl, (b) APC-0.6 M LiCl and (c) APC-0.4 M LiCl as electrolytes. (d) Reaction resistances of batteries with APC-0.2 M LiCl, APC-0.6 M LiCl and APC-0.4 M LiCl as electrolytes during discharge.

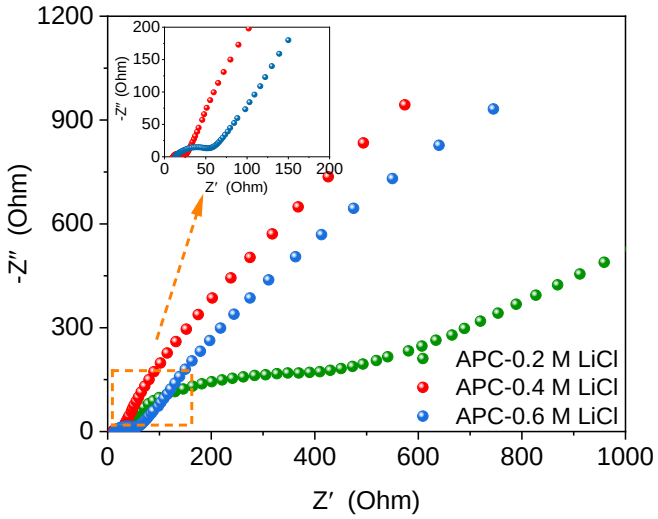

Fig. S23 EIS spectra of MLHBs with APC-0.2 M LiCl, APC-0.4 M LiCl and APC-0.6 M LiCl as electrolytes after 10 cycles at 0.2 A g^{-1}.

Table S1 Comparison on performance of MLHB with some other cathode materials and electrolytes.

Cathode materials	Electrolytes	Current density ($A\ g^{-1}$)	Cycle number	Capacity ($mAh\ g^{-1}$)	Ref.
Lamellar $SnSe_2$/SnSe/SnO_2	0.4 M APC-0.4 M LiCl	0.1	100	551	This work
		1.0	2000	233	
Mn_3O_4 nanoparticles	0.4 M APC	0.0154	30	220	[1]
Octahedral shape of Cu_2S@C	0.4 M APC-1.0 M LiCl	0.05	50	155	[2]
Lamellar Cu_2Se/CoSe	0.4 M APC-0.8 M LiCl	0.1	200	140	[3]
Flower-like CoS	0.4 M APC-0.8 M LiCl	0.1	80	457	[4]
VO_2 nanoflakes	0.25 M APC-1.0 M LiCl	0.1	100	154.9	[5]
Amorphism dilithium salt of poly(2,5-dihydroxy-p-benzoquinonyl sulfide) (Li_2PDHBQS)	1.0 M $MgCl_2$-LiCl/THF	0.5	500	166	[6]
VS_4 nanodendrites	0.4 M APC-0.4 M LiCl	1.0	1500	110	[7]
TiO_{2-x} microspheres	0.4 M APC-0.4 M LiCl	1.68	2500	91	[8]

References

[1] L. Wang, P. E. Vullum, K. Asheim, X. H. Wang, A. M. Svensson and F. Vullum-Bruer, *Nano Energy*, 2018, **48**, 227-237.

[2] W. Q. Wang, Y. Y. Yang, Y. N. Li, J. J. Zhou, J. Yang and J. L. Wang, *J. Power Sources*, 2020, **445**, 227325-227337.

[3] Z. H. Gao, R. S. Shi, Y. P. Zhao, J. G. Zhang, J. C. Liu, Y. F. Zhu, Y. N. Liu, J. Wang and L. Q. Li, *Electrochim. Acta*, 2023, **469**, 143298.

[4] X. Zhang, H. Xu, J. S. Yang, Y. X. Zhu, C. Lu, K. Zhang, G. M. Weng and J. X. Zou, Chem. *Nano Mat.*, 2021, **7**, 641-650.

[5] C. Y. Pei, F. Y. Xiong, J. Z. Sheng, Y. M. Yin, S. S. Tan, D. D. Wang, C. H. Han, Q. Y. An and L. Q. Mai, *ACS Appl. Mater. Interfaces*, 2017, **9**, 17060-17066.

[6] Y. Han, G. F. Li, Z. J. Hu, F. Wang, J. Chu, L. Huang, T. T. Shi, H. Zhan and Z. P. Song, *Energy Storage Mater*., 2022, **46**, 300-312.

[7] Y. R. Wang, C. X. Wang, X. Yi, Y. Hu, L. Wang, L. B. Ma, G. Y. Zhu, T. Chen and Z. Jin, *Energy Storage Mater*., 2019, **23**, 741-748.

[8] T. Mu, J. G. Zhang, R. Shi, Y. F. Zhu, J. L. Zhu, Y. N. Liu, Y. Zhang and L. Q. Li, *Chem. Commun*.**,** 2020, **56**, 8039-8042.